© 2017. Published by The Company of Biologists Ltd | Development (2017) 144, 4350-4362 doi:10.1242/dev.152652

RESEARCH ARTICLE

Variations in basement membrane mechanics are linked to epithelial morphogenesis

Julien Chlasta[1,*], Pascale Milani[1,*], Gaël Runel[1,*], Jean-Luc Duteyrat[2,‡], Leticia Arias[1,‡], Laurie-Anne Lamiré[1], Arezki Boudaoud[3] and Muriel Grammont[1,§]

ABSTRACT

The regulation of morphogenesis by the basement membrane (BM) may rely on changes in its mechanical properties. To test this, we developed an atomic force microscopy-based method to measure BM mechanical stiffness during two key processes in *Drosophila* ovarian follicle development. First, follicle elongation depends on epithelial cells that collectively migrate, secreting BM fibrils perpendicularly to the anteroposterior axis. Our data show that BM stiffness increases during this migration and that fibril incorporation enhances BM stiffness. In addition, stiffness heterogeneity, due to oriented fibrils, is important for egg elongation. Second, epithelial cells change their shape from cuboidal to either squamous or columnar. We prove that BM softens around the squamous cells and that this softening depends on the TGFβ pathway. We also demonstrate that interactions between BM constituents are necessary for cell flattening. Altogether, these results show that BM mechanical properties are modified during development and that, in turn, such mechanical modifications influence both cell and tissue shapes.

KEY WORDS: Basement membrane, Stiffness, Atomic force microscopy, Epithelial morphogenesis, *Drosophila*

INTRODUCTION

Extracellular matrices (ECMs) are essential for the development of multicellular eukaryotic organisms (Ozbek et al., 2010). ECM proteins form a network that fills spaces between organs and mechanically supports them (Hynes and Naba, 2012). ECMs are specialised in the cells, organs or tissues with which they are associated. For instance, epithelial sheets are found to be associated with basement membranes (BMs) and, importantly, epithelial morphogenetic processes that occur during development are known to be partly regulated by BMs. BMs control epithelial morphogenesis by providing a physical scaffold to oppose the contractile forces generated by cell shape changes, by directing growth factor delivery and by regulating cell adhesion (Hynes, 2014). All these roles depend on BM composition and structure, which in turn determine BM mechanical properties. BM mechanical properties have been shown to control cell migration *in vitro* and BM structure is modified by proteases during branching morphogenesis (Daley and Yamada, 2013; Kai et al., 2016). It is therefore essential to determine how BM mechanical properties vary *in vivo* during organ formation and to decipher the link between these properties and morphogenesis. Although ECM mechanical properties have been measured and manipulated *in vitro* in order to address their role during single-cell migration (Lo et al., 2000; Paszek and Weaver, 2004; Reinhart-King et al., 2008; Roca-Cusachs et al., 2013), it is still unknown how BM mechanical properties change during the course of development to shape cells, organs or tissues.

Here, we fill in this gap by using the ovarian follicle of *Drosophila*, which provides an ideal model to analyse the coupling between BM and tissue morphogenesis (Bilder and Haigo, 2012; Horne-Badovinac and Powell, 2015). The *Drosophila* follicle consists of an internal cluster of 16 germline cells, comprising 15 nurse cells and one oocyte, surrounded by a monolayer of epithelial cells, called follicle cells, that are in contact with an external BM (Fig. 1A,B). Follicles are linearly and chronologically arranged in ovarioles. Follicles are formed in the most anterior structure of the ovariole, called the germarium. Germaria enclose germline and somatic stem cells and produce follicles during the entire lifetime of the fly. Follicles mature progressively toward the posterior. Their maturation has been divided into 14 stages, with stage 1 corresponding to a fully formed follicle leaving the germarium and stage 14 to a mature egg (King, 1970). The BM that surrounds the germarium and the follicles is composed of the core BM proteins and so typically consists of Laminin, the glycoprotein Nidogen, the heparan sulphate proteoglycan Perlecan (Pcan, also called Trol) and Collagen IV (Coll IV), which itself comprises helical trimers of three α chains (Yurchenco, 2011). BM components interact with the epithelial cells through Integrin and Dystroglycan receptors. BM components are produced by the follicular cells, by the fat body, which is the metabolic organ in insects, and by some companion blood cells called hemocytes that lie closed to the germarium (Van De Bor et al., 2015).

During follicle development, the epithelial cells undergo two main morphogenetic processes: first, they migrate collectively around the anteroposterior (A/P) axis within the static BM from stage 2 to late stage 8; and second, they change shape from cuboidal to either squamous or columnar during stage 9. At present, it is established that BM structure changes during rotation (Cetera et al., 2014; Haigo and Bilder, 2011; Isabella and Horne-Badovinac, 2015b). During the rotation, the follicular cells deposit BM components in linear 'fibril-like' structures that are perpendicular to the A/P axis (Fig. 1C) (Isabella and Horne-Badovinac, 2016). These BM fibrils are proposed to establish an anisotropic stiffened corset, which forces the initially spheroid follicles to elongate

[1]Laboratoire de Biologie et de Modélisation de la Cellule, Université de Lyon, ENS de Lyon, UCB Lyon 1, CNRS, F-69342, Lyon, France. [2]Institut NeuroMyoGene, Université Claude Bernard Lyon 1, CNRS UMR 5310, INSERM U1217, 16 rue R. Dubois, Villeurbanne Cedex F-69622, France. [3]Laboratoire Reproduction et Développement des Plantes, Université de Lyon, ENS de Lyon, UCB Lyon 1, CNRS, INRA, F-69342, Lyon, France.
*These authors contributed equally to this work
‡These authors contributed equally to this work

§Author for correspondence (muriel.grammont@ens-lyon.fr)

J.-L.D., 0000-0002-7126-8798; A.B., 0000-0002-2780-4717; M.G., 0000-0002-9693-2181

Received 24 March 2017; Accepted 5 October 2017

Development (2017) 144, 4350-4362 doi:10.1242/dev.152652

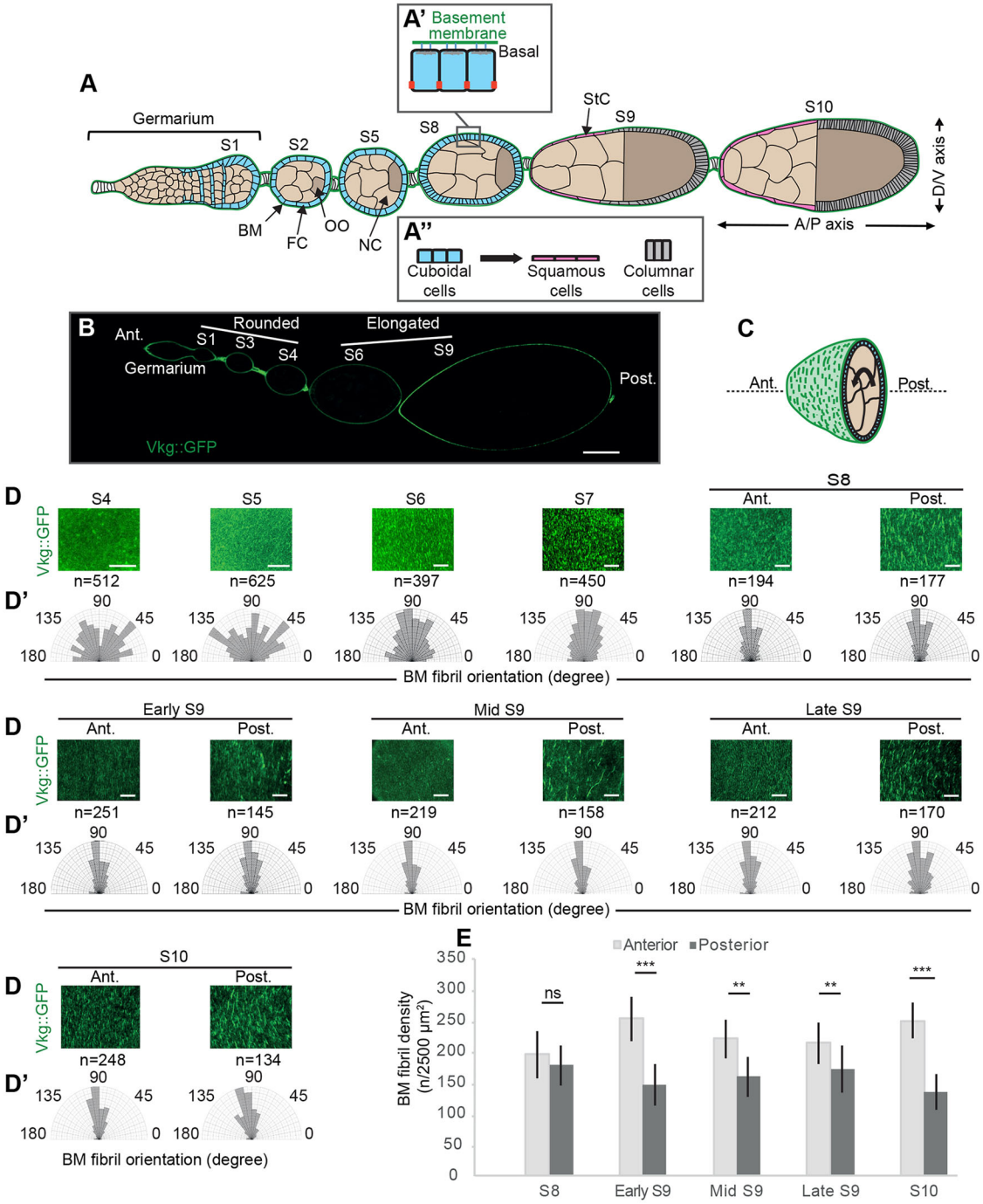

Fig. 1. BM fibrils are remodelled during cell shape changes. In all figures, anterior (Ant.) is to the left; posterior (Post.) to the right. (A) Schematic representation of an ovariole with a germarium and follicles at different stages (S) and of epithelial cell polarity (A′) and cell shape changes (A″). The arrangement and identities of the oocyte (OO; dark brown), nurse cells (NC; light brown), main body follicular cells (FC; blue), stretched cells (StC, red) and columnar cells (grey) are shown. A basement membrane (BM; green) surrounds the germarium and the follicles. A/P, anteroposterior axis; D/V, dorsoventral axis. (B) Ovariole with the BM (green) containing Vkg::GFP. (C) Schematic representation of follicle rotation. (D) BM with puncta or fibrils from stage 4 to stage 10. Images were taken with identical microscope settings. Scale bars: 10 µm. (D′) Measurements of fibril orientation relative to the A/P axis: the length of the bars represents the total number of fibrils at each range of angles. *n*, number of fibrils per 2500 µm^2. (E) Change in fibril density from stage 8 to 10 (for D and E, five follicles per stage were used). Error bars indicate s.e.m. ns, not significant; ***P*<0.01, ****P*<0.005, *t*-test.

progressively along the A/P axis after stage 5 (Bilder and Haigo, 2012; Haigo and Bilder, 2011). Links between BM components and follicle elongation have been demonstrated through analyses of the role of the α2-chain of Coll IV, which is encoded by *viking* (*vkg*), and of the βPS subunit of Integrin, encoded by *myospheroid* (*mys*). Mutations in these genes cause rounded eggs to be produced (Haigo and Bilder, 2011). Recently, it has been shown that the BM is stiffer near the centre of the follicle than at the extremities (Crest et al., 2017), suggesting that elongation is favoured by the softer BM at the poles. However, the significance of fibril incorporation, its stiffness and spatial organisation is still unknown. The second main morphogenetic process that occurs during follicle development

Development (2017) 144, 4350-4362 doi:10.1242/dev.152652

starts as soon as the rotation stops. The cells change their shape: ∼50 anterior follicle cells flatten around the nurse cells while all the others become columnar around the oocyte (Fig. 1A) (King, 1970). So far, no link has been demonstrated between these cell shape changes and the BM. However, such links are likely to exist, as cell flattening involves increasing the basal surface and thus modification of the interactions with the BM. In addition, previous data have shown that *decapentaplegic* (*dpp*), which belongs to the TGFβ superfamily, controls cell flattening in this system (Brigaud et al., 2015), and studies in vertebrates have described the role of the BM in TGFβ activity (Saika et al., 2001). Thus, measuring local BM mechanical properties from stage 2 to stage 10 should provide valuable information to help decipher the link between BM and epithelial morphogenesis.

To investigate this link, we designed an atomic force microscopy (AFM) approach to measure the stiffness of the BM in living ovarian follicles at different stages of development in wild type (WT) and in several mutant conditions that disrupt BM structure. Our results show that BM stiffness increases while the follicle rotates, and reveal stiffer fibrils. We also demonstrate that the formation of fibrils is important to spatially organise BM mechanical properties. We then combined this approach with classical genetic analyses to demonstrate the link between BM stiffness and epithelial cell flattening. We found that the BM becomes soft around the cells that flatten and that TGFβ activity is responsible for this softening.

RESULTS

BM fibril-like structures are remodelled during epithelial cell shape changes

During follicle rotation, it has been shown that the deposition of Coll IV (visible by using the vkg^{G454} allele, termed Coll IV::GFP or Vkg::GFP) around the follicles increases and that the density, the length and the orientation of the fibril-like structures evolve from stage 4 to 12 (Haigo and Bilder, 2011). However, no analysis has been carried out specifically at stage 9, when follicle cells change their shape from cuboidal to either squamous or columnar. We analysed the density and orientation of the fibrils from stage 2 to stage 10, with a focus on stage 9. We first confirmed that Coll IV::GFP expression levels increase between stages 4 and 7 (Fig. S1A) and that fibrils are mostly oriented perpendicular to the A/P axis from stages 8 to 10 (Fig. 1D). Second, we observed that the size and density of the fibrils differ between the anterior and posterior half of the follicles from stage 8 to 10. The fibrils are shorter and denser in the anterior than in the posterior (Fig. 1D,E, Fig. S1B,C). Thus, our data reveal that the BM undergoes major modifications when the rotation stops and that these modifications differ according to the shape of the epithelial cell localised beneath. This suggests that BM mechanical properties are temporally and spatially regulated during follicle development.

Several studies suggest that fibrils make a corset around the follicle to force its elongation along the A/P axis (Bilder and Haigo, 2012; Haigo and Bilder, 2011). We treated stage 10 follicles with collagenase to determine whether the differences in fibril size and density between the anterior and the posterior of the follicles act to differently constraint follicle shape. We observed that the anterior and posterior parts of the follicles round up. This confirms that the BM is essential to shape the follicle and suggests that both short and long fibrils can generate a corset (Fig. S1D, Movie 1). Additionally, although some fibrils are still observed after 60 min of collagenase treatment, major tears spanning the circumference of the follicle appear and epithelium discontinuity is visible at the interface between the stretched and the columnar cells, inferring local differences in stiffness between the two parts of the follicle (Fig. S1E-H).

A method to measure BM stiffness in live ovarian follicles using AFM

A standard approach to measure mechanical properties of biological samples is the use of AFM (Fig. 2A). We established a method to measure the elastic modulus of the BM on live follicles. The elastic modulus quantifies how easily an elastic material is deformed when a force is applied to it; a high value of modulus corresponds to a stiff material.

Follicles are dissected in live imaging medium and the muscular sheet is manually removed. Follicles are placed on Petri dishes coated with poly-L-lysine filled with the live imaging medium at room temperature. To obtain quantifications of BM stiffness, we analysed the raw force curves given by the AFM with the protocol developed by Milani et al. (2011, 2014) (see Materials and Methods for details; Fig. 2B,C). The stiffness of the cantilever and the force applied were chosen to enable indentation of the BM with little deformation of the underlying tissues (Fig. 2D). To determine which range of indentation depths gives the elastic modulus of the BM, we first measured the thickness of the BM at different stages of oogenesis using transmission electron microscopy (TEM). The BM depth varies from 80 nm at stage 6 to 180 nm at stage 10 (Fig. 2E,F). We noticed that at stage 10 the BM above the columnar cells is thicker than that above the squamous cells. Second, we obtained topographic images of decellularised BM lying on a slide using the PeakForce QNM mode of the AFM. This mode can be used either to record surface topology or to create a map of the BM elastic modulus. We measured a difference of height between the glass and the BM of 120±20 nm at stage 10 (Fig. 2G), consistent with TEM data. Third, we determined the stiffness of the follicle as a function of the indentation depth, because the apparent elastic modulus may change due to the deformation of the successive layers beneath the surface of the sample. To do so, the measurement was performed with the Contact mode (Ramp module) of the AFM, which registers 100 raw force curves from a 10×10 matrix, with indentation points spaced 150 nm apart (Fig. 2H,I). BM stiffness was calculated in stage 8 follicles for indentation depths of up to 600 nm. We observed that the values of elastic modulus are independent of depth, as long as the depth is less than 100 nm (Fig. 2J). From all these results, we decided to perform all measurements of BM stiffness with an indentation depth of 50 nm, which is smaller than BM thickness.

Finally, the fact that these measurements were performed on living WT follicles means that the BM is likely to be under tension from the follicular and germline cells and, therefore, that the measured elastic modulus in fact represents an apparent modulus. To estimate this tension, we treated stage 7 follicles with a pharmacological inhibitor of Rho kinase (Y-27632), which has been shown to inhibit Myosin activity in follicle cells (He et al., 2010). No significant differences were observed after treatment, indicating that measurements at 50 nm indentation reflect mainly BM stiffness (Fig. 2K).

BM stiffness increases while the follicles rotate

To determine the apparent elastic modulus during follicle development, we analysed raw force curves from the middle of the follicle for stages 2 to 10. We observed that stiffness increases gradually until stage 7, before it rises rapidly to 800±200 kPa at stage 8 (Fig. 3A). Analyses of the 100 raw force curves at each region measured show that the variability of the BM stiffness also

Development (2017) 144, 4350-4362 doi:10.1242/dev.152652

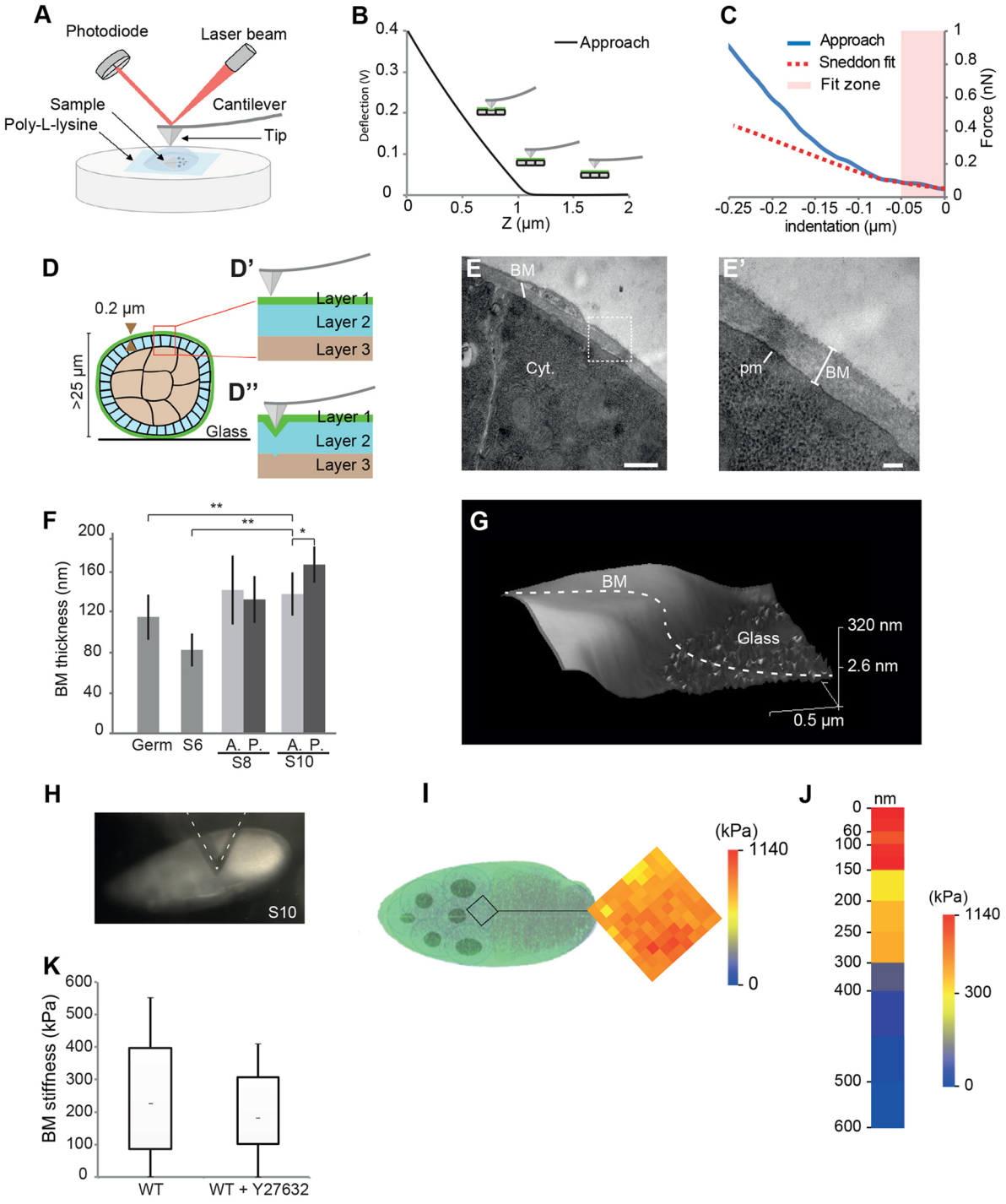

Fig. 2. Method to measure BM stiffness in live follicles. (A) The set-up used to obtain force curves with AFM. (B) A typical deflection Z curve (approach) obtained from the follicle. Z describes the motion of the cantilever towards the sample; the 0 position on this axis is determined empirically by the user, and corresponds to the bending of the cantilever for a deflection maximum imposed by the user. As the surface resists penetration, the cantilever bends and a deflection is recorded. (C) Force-indentation depth curve (blue) obtained on a follicle using a pyramidal probe tip. The curve is fitted using the Sneddon model (red dotted line) to obtain the value of the elastic modulus. Only the zone of interest (50 nm) is fitted. (D) Schematic representations of a stage 2 follicle (D) and of a shallow (D′) or deep (D″) indentation. (E) Electron microscopy of a stage 8 follicle. E′ is a magnified view of the boxed region in E. Cyt., cytoplasm; pm, plasma membrane. Scale bars: 500 nm in E; 100 nm in E′. (F) Change in BM depth during oogenesis [six images per follicle (n=3) per condition]. Error bars indicate s.e.m. *P<0.05, **P<0.01, t-test. Germ, germarium; A., anterior; P., posterior. (G) Topographic map of BM from a decellularised follicle. A nonlinear scale is used for the z-axis. (H) Follicle with the cantilever (dotted white line) located at the boundary between the StC and columnar cells. (I) Sample representation of a stiffness assay in a late stage 9 follicle. The black box indicates the probed area, which consists of a 10×10 matrix with indentation points spaced 150 nm apart. The 100 measurements are represented using a colour-coded grid with a specific colour scale (see Materials and Methods). (J) Colour-coded representation of follicle stiffness as a function of indentation. For each indentation step, 100 force-indentation curves were analysed (n=3). (K) BM stiffness from WT follicles (n=10) or from follicles after Rock kinase inhibitor treatment (n=6). In all box and whisker plots, boxes extend from the 25th to 75th percentile, with a line at the median. Whiskers extend to the most extreme values.

Development (2017) 144, 4350-4362 doi:10.1242/dev.152652

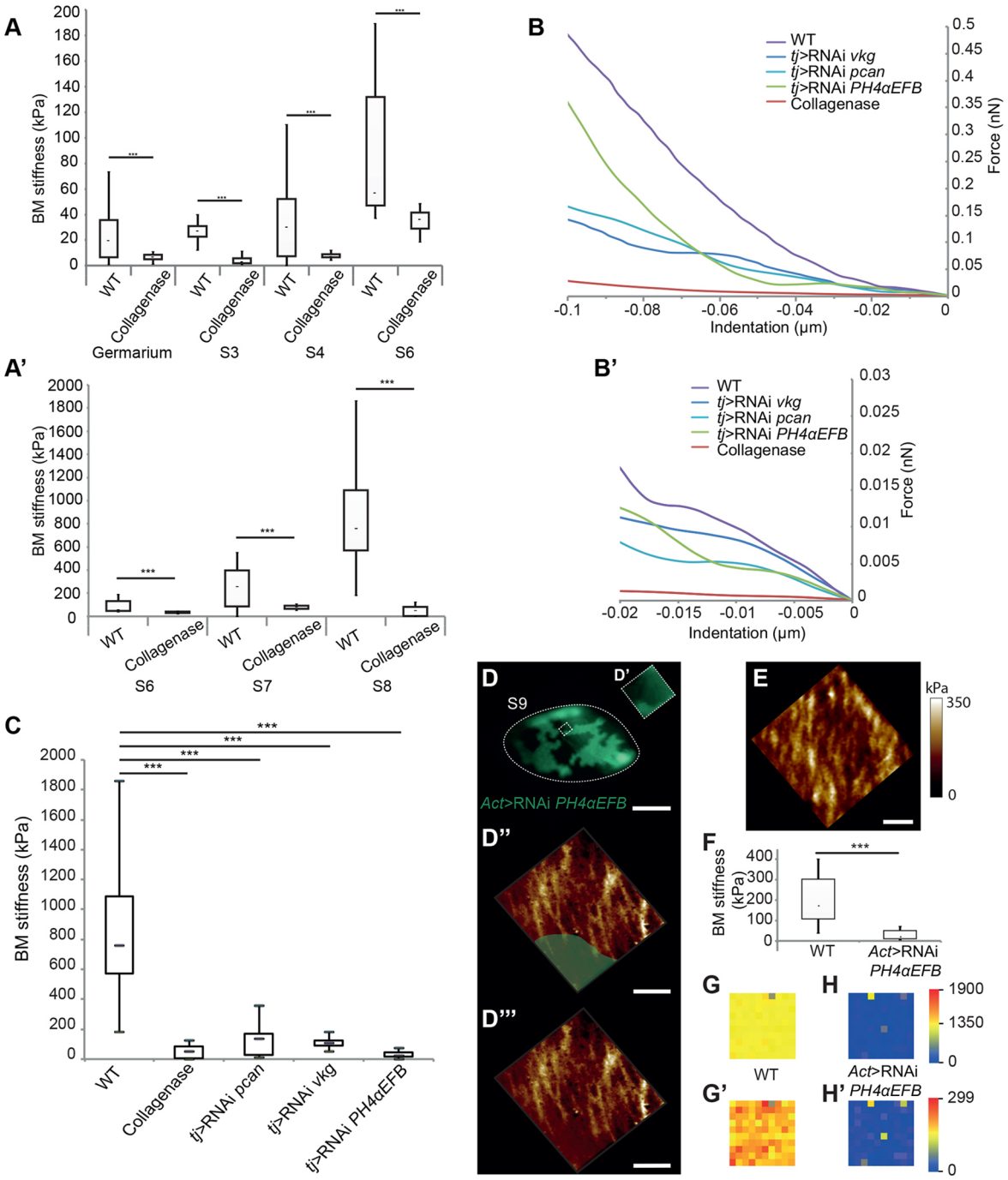

Fig. 3. BM stiffness increases from stage 2 to stage 8. (A) Box and whisker plots of BM stiffness from WT follicles or from follicles after collagenase treatment (*n*=8 per stage per condition). A different scale is used in A and A′. (B-C) Force-indentation curves (B) or box and whisker plots (C) of BM stiffness from stage 8 WT follicles or those with a genetically or mechanically impaired BM. B′ is a magnified view of the first 20 nm of indentation in B (*n*=5 for each condition). (C) BM stiffness for an indentation depth of 50 nm. (D) Follicle with cells expressing RNAi against *PH4αEFB*. D′ is a magnified view of the boxed region. D″ and D‴ represent the elastic modulus map of a part of the boxed region with (D′) or without (D″) the delimitation of the clone (green shading). (E) Elastic modulus map of an equivalent area from a WT stage 9 follicle. The colour gradient allows the visualisation of differences in stiffness from weak (black) to strong (white). Scale bars: 50 μm in D; 1.5 μm in D″,D‴; 1 μm in E. (F-H) Box and whisker plots (F) or matrices with a common (G,H) or specific (G′,H′) scale of BM stiffness from WT areas (*n*=6) or from areas expressing RNAi against *PH4αEFB* (*n*=4) in mosaic follicles. ***P<0.005, *t*-test.

increases at stages 7 and 8 (Fig. 3A). This suggests that the BM structure is non-uniform, which is consistent with fibrils being incorporated within the BM from stage 5 onwards (Isabella and Horne-Badovinac, 2016).

We then analysed the stiffness in different mutant conditions that alter the structure and/or composition of the BM. All mutant conditions led to a decrease in the fluorescence intensity of Coll IV::GFP or Pcan::GFP by a factor of two to four (Fig. S2A,B, Movie 2). First, we incubated follicles with collagenase, which cleaves the triple helix, and observed an immediate decrease in stiffness at all stages of follicle development, indicating that Coll IV integrity is important for BM mechanical properties (Fig. 3A-C, Fig. S2C).

Development (2017) 144, 4350-4362 doi:10.1242/dev.152652

Second, the effect of reduced levels of Coll IV in the BM was assessed by analysing follicles expressing RNAi against *vkg* or against the procollagen *prolyl-4-hydroxylase-alpha EFB* (*PH4αEFB*) under the specific follicle cell *traffic jam* (*tj*)-Gal4 driver. PH4αEFB is required for Coll IV trimer assembly and stability, and thus knockdown of this enzyme prevents Coll IV from being secreted (Myllyharju and Kivirikko, 2004) (Fig. S2D). Before AFM measurement, we determined BM thickness by electron microscopy. *vkg* mutant follicles have a BM that is less dense but thicker (300±50 nm) than that of WT follicles, whereas the BM around *PH4αEFB* mutant follicles is of normal thickness (160±30 nm) (Fig. S2E-G). These data indicate that our protocol, with an indentation depth of 50 nm, can be used to determine BM stiffness in these mutants. Analyses of raw force curves showed a reduction of BM stiffness for this indentation depth as well as for smaller indentations (<20 nm; Fig. 3B,C, Fig. S2C). Third, we measured the stiffness of follicles expressing RNAi against *pcan* and also observed a reduction in stiffness (Fig. 3B,C, Fig. S2C). This reduction is detectable for indentation depths that are less than 25 nm. This experiment indicates that the Pcan expression level is important for BM stiffness, but as *pcan* follicles have a thin BM with signs of degradation it is too delicate to assign a stiffness value to this mutant (Fig. S2H). Similar caution is required when considering BM stiffness measurements following collagenase treatments.

Finally, we also mapped the elastic modulus at the interface of WT and cells expressing RNAi against *PH4αEFB*. Owing to the rotation of the follicle from stage 2 to 8, we expected to observe a reduction in BM stiffness all around the follicle and not specifically just above the mutant cells. In such follicles, the BM is indeed less stiff than WT BM (compare Fig. 3D with 3E). However, the BM above the mutant clone is also softer than the BM above the neighbouring WT cells (compare Fig. 3D″ with 3D‴, Fig. S2I), indicating that BM remodelling is dynamic since local differences in stiffness between WT cells and cells impaired in BM production can be detected soon after the rotation stops. Quantifications of BM stiffness above exclusively WT or exclusively mutant areas show a decrease in stiffness by a factor of four (Fig. 3F-H).

Altogether, these results show that BM mechanical properties depend on BM composition and structure and demonstrate that BM stiffness increases while the follicles rotate.

Fibril-like structures stiffen the BM

The BM structure of the ovarian follicle contains fibrils that are produced by the follicular cells and that are progressively embedded in the BM during rotation (Isabella and Horne-Badovinac, 2016). As these structures are supposed to add rigidity to the corset around the follicles, we used the QNM mode of the AFM to probe the surface of the BM and determine the stiffness of these structures. First, with the topographic map on live follicles we observed fibrils with similar length, width and orientation as those seen in fluorescence microscopy (Fig. 4A,B). Second, this representation also allowed us to observe, on decellularised BM, that the BM surface is uneven, with protruding structures localised at the same position as the fibrils (compare Fig. 4C with 4Ca). Third, we generated an elastic modulus map of the same decellularised BM and demonstrated that areas with fibrils are stiffer than the surrounding regions (Fig. 4Cb). Fourth, matrices on live stage 8 follicles occasionally reveal stiff structures of a size and orientation similar to the fibrils observed by confocal microscopy (Fig. 4D). Such structures are detected only in matrices from stage 7 onwards. Importantly, analyses of the matrices without any detectable fibrils from stage 4 to stage 8 show that the increase in BM stiffness is not only due to the incorporation of the fibrils (Fig. 4E-H). Altogether, these results show that fibril incorporation enhances BM stiffness locally, but that the BM stiffness increase is global.

The deposition of new BM materials in fibrils is due to the rotation of the follicles. In the absence of rotation, such as in a *fat2* (*kugelei*) mutant, BM materials are still deposited basally but in ring-like aggregates around the cells, with small ridges overlaying the cells (Isabella and Horne-Badovinac, 2016; Squarr et al., 2016; Viktorinová et al., 2009). To determine whether the incorporation of BM materials with a fibril shape is essential for stiffness, we measured the BM of a *fat2* mutant follicle. On average, the BM of *fat2* follicles is more rigid than in the WT. However, the stiffness is highly variable and this variability can be observed between matrices as well as within matrices. Some curve forces give an elastic modulus lower than WT, whereas others show an elastic modulus 10% higher than WT (Fig. 4I-L). QNM-based modulus maps of stage 8 *fat2* follicles show highly heterogeneous BM, with seemingly hexagonal stiffness patterns. The width of these hexagonal elements (~6 µm) suggests that they might correspond to the accumulation of BM materials in the intercellular space between adjacent cells (Fig. 4M,N). Finally, we measured BM stiffness on decellularised *fat2* follicles using 10×10 matrices. We confirmed that *fat2* BM is stiffer and more heterogeneous than that of WT (Fig. 4O).

Altogether, these data show that rotation is important for the proper spatial organisation of the mechanical properties of the BM into alternating soft and oriented stiff areas. This indicates that round eggs in *fat2* mutants are not due to lack of a stiff BM around the follicle and that BM organisation with fibrils is likely to be important for egg elongation.

Local BM mechanical properties are controlled by TGFβ signalling

We showed that BM is remodelled from stage 9 onwards with variations of fibril size and density between the anterior and the posterior parts of the follicle (see Fig. 1D,E). During this stage, ~50 stretched cells (StCs) flatten progressively from the anterior to the middle of the follicle, whereas the others become columnar around the oocyte (Fig. 1A).

To determine whether changes in BM structure correlate with changes in BM stiffness, matrices were measured along the A/P axis. If follicles had developed sufficiently, four areas (1, 2, 3 and 4) were probed that correspond to flattened cells, flattening cells, unflattened cells overlying the nurse cells, and columnar cells overlying the oocyte, respectively. Otherwise, only areas 2, 3 and 4 were measured as it is difficult to obtain representative matrices at the highly curved extremity of the follicle (Fig. 5A,B). The analyses of curves showed that the stiffness decreases in the anterior during cell flattening, whereas it increases in the posterior (Fig. 5C, Fig. S3A,B), indicating that a gradient of stiffness from anterior to posterior is established during cell shape changes. At stage 10, BM stiffness above the StCs is on average one-tenth of that above the columnar cells (Fig. 5C, Fig. S3A,B). Some stiff fibrils are still detected. Areas with or without fibrils are less stiff than those at stage 8 (Fig. S3B). This indicates that BM stiffness correlates with BM remodelling, but that stiffness cannot be deduced by analysing only the size and the density of the visible fibrils. This stiffness is also dramatically reduced when follicles are mutant for *vkg*, *pcan* or after collagenase treatment (Fig. S3C). We also observed an abrupt variation in stiffness around the junction between the StCs and the columnar cells, suggesting a link between changes in BM stiffness and cell shape (Fig. 5D).

Development (2017) 144, 4350-4362 doi:10.1242/dev.152652

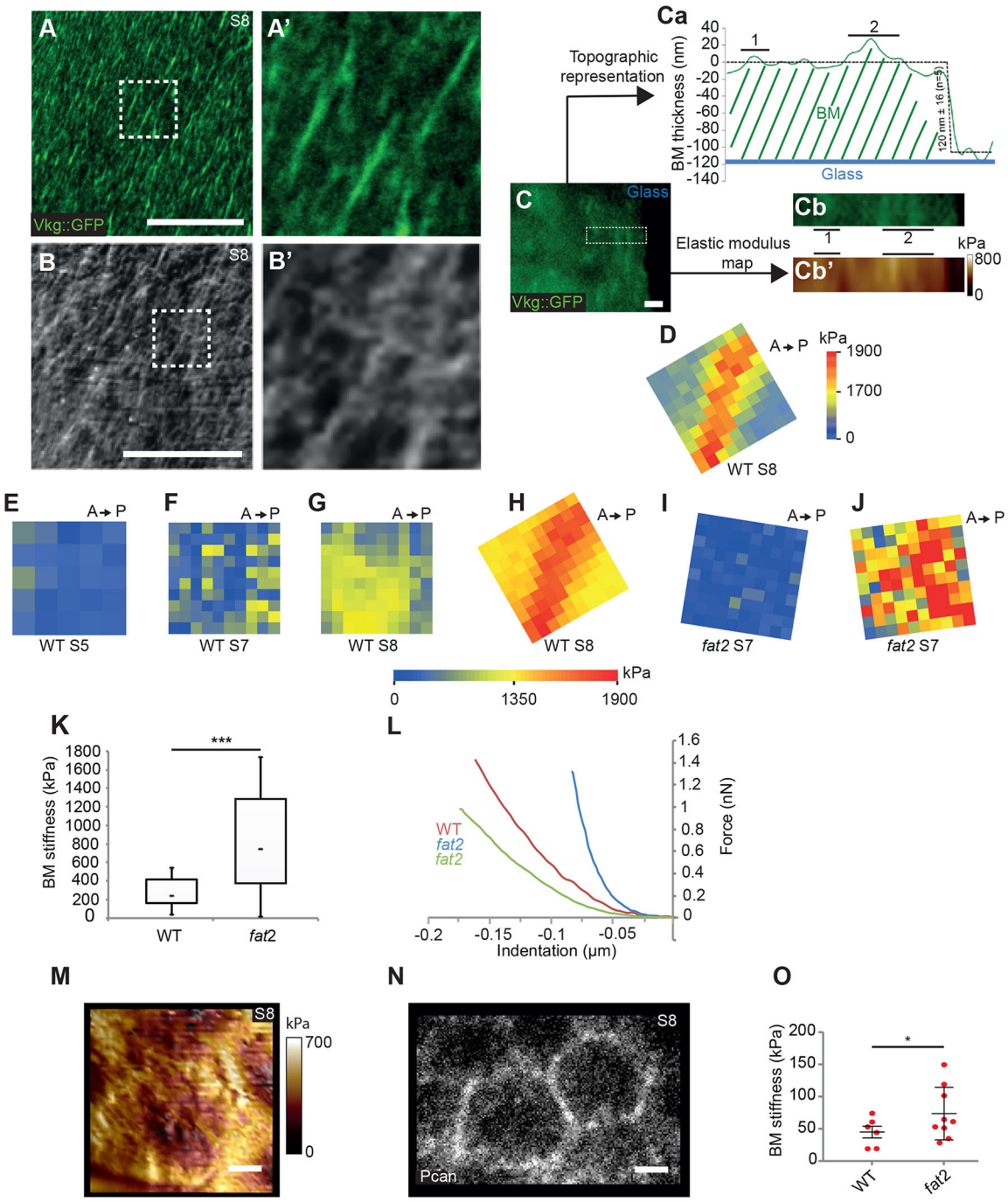

Fig. 4. Fibrils stiffen locally the BM. (A) BM with fibrils. (B) Topographic map of a BM (*n*=2). (A′,B′) Magnified views of the boxed regions in A and B. (C) BM fragment with fibrils from a decellularised follicle. Ca is a topographic representation of the BM surface from a line positioned in the middle of the boxed region in C. Cb is a magnified view of the boxed region in C. Cb′ is the elastic modulus map of this boxed region. 1 and 2 correspond to the protruding areas detected in Ca. (D) Matrix of BM stiffness with a specific scale (*n*=5). (E) 5×5 matrix of BM stiffness with each indentation point spaced 300 nm apart and the common scale (*n*=5). (F-J) Matrices of BM stiffness with the common scale. (F) BM area of a stage 7 follicle (*n*=10). (G,H) BM area of a stage 8 follicle that contains (H, *n*=3) or does not contain (G, *n*=10) visible fibrils. (I,J) BM areas from two stage 7 *fat2* mutant follicles (*n*=16). (K,L) Box and whisker plots (K) or force-indentation curves (L) of BM stiffness from stage 7 WT (*n*=10) or *fat2* (*n*=16) follicles. (M) Elastic modulus map of an area from a *fat2* follicle (*n*=4). (N) Pcan expression in a *fat2* follicle. (O) Decellularised BM stiffness in stage 7 WT (*n*=6) and *fat2* (*n*=9). Red dots represent individual values. Error bars indicate s.e.m. **P*<0.05, ****P*<0.005, *t*-test. Scale bars: 10 µm in A,B; 1 µm in C,M,N.

To test this hypothesis, we first analysed Pcan, Coll IV::GFP, Laminin B1::GFP and endogenous Rab10::YFP expression in WT in StC and columnar cells. All the BM components and Rab10 are expressed by the two types of cells (Fig. S4A), indicating that the decrease in BM stiffness above the StC is not due to lack of BM material production and deposition by these cells.

Second, we analysed the stiffness in two mutant conditions that disrupt cell shape change. We have previously shown that cell flattening is controlled by the Dpp/BMP pathway (Brigaud et al.,

Development (2017) 144, 4350-4362 doi:10.1242/dev.152652

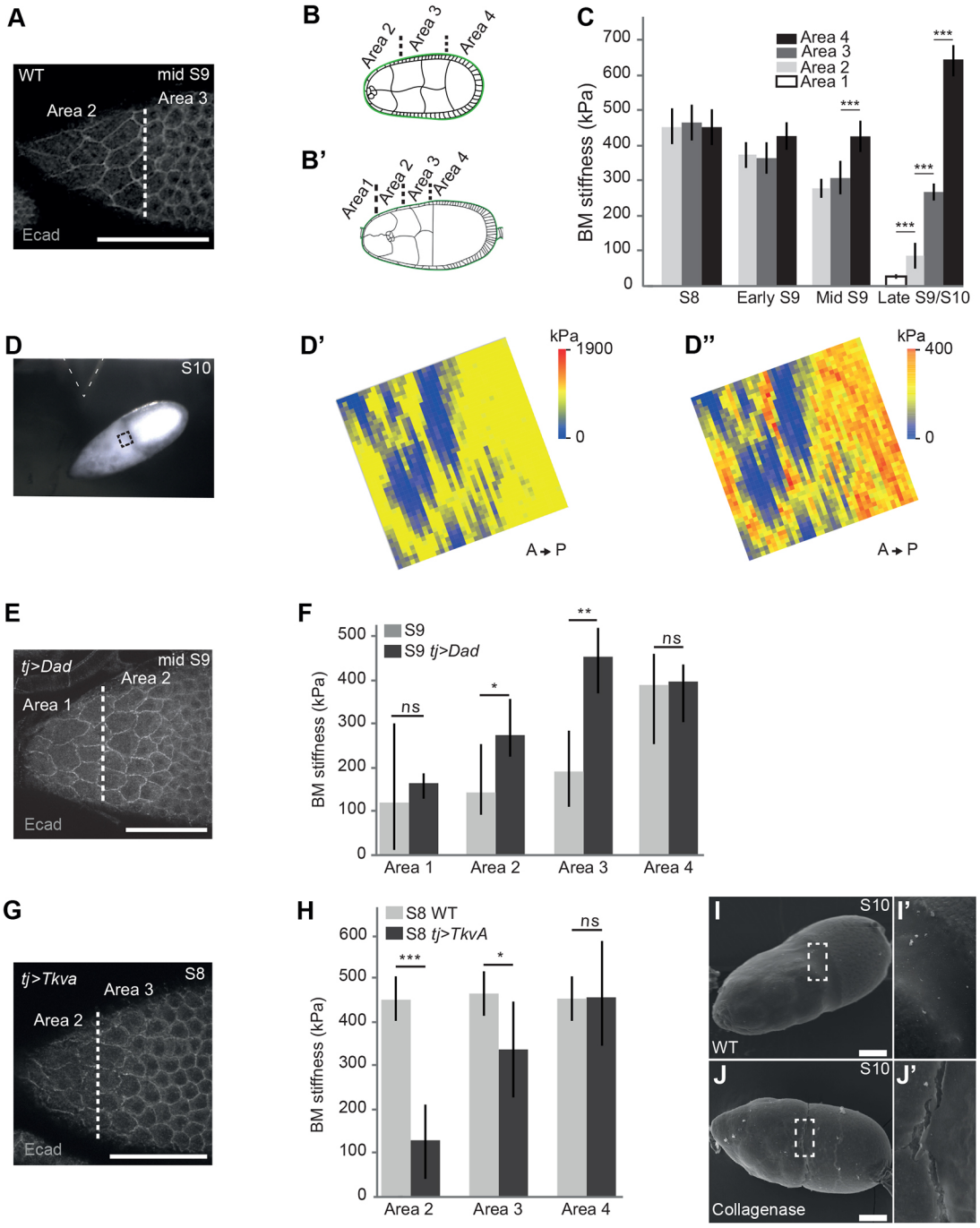

Fig. 5. Cell flattening controls BM stiffness locally. (A) Mid stage 9 WT follicle stained for E-cadherin, showing the delineation of areas 2 and 3. (B,B′) Schematic representation of the measured areas on an early stage 9 (B) and a late stage 9 (B′) follicle. (C) Changes in BM stiffness from stage 8 to stage 10 for each area (n=10 follicles per stage). (D) WT follicle. The boxed region represents roughly the position of the 40×40 matrix of BM stiffness presented in D′ (common scale) and D″ (specific scale), with each indentation point spaced 50 nm apart. (E) Follicle expressing Dad. (F) BM stiffness of WT follicles and of follicles expressing Dad at late stage 9 (n=4). (G) Follicle expressing TkvA. (H) BM stiffness of WT follicles and of those expressing TkvA at stage 8 (n=5). (I,J) Scanning electron micrographs of stage 10 WT follicles with and without collagenase treatment (n=3). (I′,J′) Magnified views of the boxed regions in I and J. Error bars indicate s.e.m. *P<0.05, **P<0.01, ***P<0.005, t-test. Scale bars: 50 µm.

2015). In *Drosophila*, Dpp binds to a heteromeric receptor complex composed of at least the type I Thickveins (Tkv) protein and the type II Punt protein. Activation of the pathway leads to the transcription of target genes, such as *Daughters against dpp* (*Dad*), which then negatively regulates the pathway. We analysed the BM in follicles that overexpress either Dad or a constitutively active form of Tkv termed TkvA. In the first mutant condition, cell flattening is delayed, whereas in the second condition cell flattening occurs prematurely. In follicles overexpressing Dad, we performed the experiment in late stage 9 follicles. The BM in areas 1, 2 and 3 is stiffer than in the corresponding WT areas, indicating that TGFβ activity is required for BM softening at stage 9 (Fig. 5E,F, Fig. S3D). We then performed similar experiments in stage 8 TkvA-expressing follicles as flattening starts precociously. As follicles are

Development (2017) 144, 4350-4362 doi:10.1242/dev.152652

smaller than those at stage 9 and 10, only areas 2, 3 and 4 were probed. We detected that the BM in areas 2 and 3 is softer than in the corresponding WT areas at stage 8, indicating that premature TGFβ signalling is sufficient to induce BM softening (Fig. 5G,H, Fig. S3E). Importantly, the BM overlying the columnar cells in Dad-overexpressing or TkvA-expressing follicles remains as stiff as in WT, indicating that this role of TGFβ activity is specific to StCs.

Third, we analysed fibril shape in these mutant conditions. At the end of stage 8, fibrils in the anterior part of TkvA-expressing follicles are shorter and thinner than in the WT, whereas fibrils of Dad-overexpressing follicles are longer than in the WT (Fig. S5A-E). Altogether, these data show that TGFβ locally controls BM stiffness and remodelling.

To further investigate BM mechanical properties, we treated follicles with collagenase and observed them by scanning electron microscopy. The major tears at the boundary between the StC and columnar cells are consistent with the large difference in stiffness between the two sides (Fig. 5I,J). Some tears are also present above the StC and halfway through the posterior part of the follicle. These results confirm that BM mechanical properties differ locally from stage 9 onwards.

Finally, we measured BM stiffness in *fat2* mutant follicles. Because of the shape and size of *fat2* follicles, it is difficult to distinguish areas 1, 2, 3 or 4. The first probed area is likely to be composed of flattened and flattening cells (areas 1 and 2), whereas the second is expected to contain unflattened cells overlying the nurse cells, as well as columnar cells overlying the oocyte (areas 3 and 4). The anterior area presents a BM stiffness similar to that of areas 1 and 2 of late stage 9 WT follicles. The central area is as stiff as area 4 of late stage 9 WT follicles (compare Fig. S5F,G with Fig. 5C). These data show that TGFβ activity controls local BM softening in the *fat2* mutant, as it does in the WT.

Cell flattening depends on interactions between the BM and basal adhesion molecules

We then investigated whether, in turn, interactions between the StC and the BM are important for cell flattening. We examined adherens junction remodelling under collagenase treatment or in mutants that disrupt BM structure and measured apical surface, shape and flattening orientation (Brigaud et al., 2015; Grammont, 2007). After 20 min of collagenase treatment, adherens junctions exhibit an abnormal pattern of disassembly, with a lack of junctions between flattened cells and cells undergoing flattening during mid-stage 9. This phenotype can already be observed at 10 min for late stage 9 follicles. At stage 10, some StC nuclei are positioned between, rather than above, the nurse cells and the epithelium appears discontinuous between the StC and the columnar cells (Fig. S6). These data show that the integrity of BM structure is important during cell flattening.

Analyses of follicles with clones for a null allele of *vkg*, or clones expressing RNAi against *PH4αEFB*, show that the mutant cells present a smaller apical surface than WT cells, that remodelling of their adherens junctions is delayed compared with WT, and that they are not well elongated along the A/P axis (Fig. 6A-E). These data show that production of Coll IV is important to control cell flattening. Importantly, the detection of abnormal flattening in cells impaired for Coll IV synthesis or secretion shows that BM remodelling continues after rotation ends.

Follicles with cells mutant for a null allele of *mys*, which encodes the sole Integrin β-subunit (βPS) expressed during follicle development (Fernández-Miñán et al., 2007), or with cells expressing RNAi against *Focal adhesion kinase* (*Fak*), present similar phenotypes (Fig. 6F-I). Thus, cell flattening depends on interactions between the basal side of the epithelial cells and the BM.

DISCUSSION

BMs are known to assist epithelial cells during morphogenetic processes by providing a mechanical support to resist the contractile forces emanating from epithelial cells, by constraining locally or globally the expansion of tissues, by regulating growth factor delivery, and by regulating cell adhesion and signalling of BM receptors (Daley and Yamada, 2013; Hynes, 2014; Kai et al., 2016). A growing body of evidence shows that BM structure, and therefore BM mechanical properties, is remodelled during development, and that BM stiffness tunes epithelial morphogenesis (Tse and Engler, 2011; Wei et al., 2015). In our study, we measured BM stiffness during two epithelial morphogenetic processes of follicle development: collective cell migration from stage 2 to 8, and cell shape changes at stage 9. We first developed an AFM-based protocol to determine BM stiffness. We observed that BM stiffness increases progressively during the rotation of the follicle before rising abruptly at stage 7/8. We demonstrate that BM structure is important for its stiffness and that BM with fibrils is stiffer than that around them. We show that collective cell migration allows the formation of alternate soft and oriented stiff areas that are important for egg elongation. Our study also reveals that BM stiffness is later locally modulated around the cells undergoing the cuboidal-to-squamous transition and that this softening depends on TGFβ signalling.

AFM is an efficient technique to measure local stiffness in living tissue. This has been successfully used to probe the hypocotyls of seedlings and shoot apical meristems in *Arabidopsis*, and BM in glial migration or in the corneal lens in *Drosophila* (Kim et al., 2014; Lavanya Devi et al., 2016; Milani et al., 2011, 2014). One challenge for this technique is to determine the correct indentation to measure the mechanical properties of a layer in multi-layered tissues. In our system, we showed that the stiffness varies as a function of indentation but is stable as long as the probe does not indent more than half of the depth of the layer. These results are in accordance with previous analyses showing that indentions of about one-third of the depth of the layer give the stiffness of that layer (Milani et al., 2011). In two studies showing AFM measurements of BM stiffness in follicles, the measured stiffness is ten times softer than in our analyses, but with a deeper indentation (200 nm) (Diaz de la Loza et al., 2017; Pearson et al., 2016). This is consistent with our observations that stiffness decreases as indentation depth increases. Their values cannot directly be compared with ours because they used a large spherical probe (5 µm diameter), giving global measurements, whereas we used a thin pointed tip, allowing the detection of BM stiffness heterogeneity. Importantly, although our method gives local measures, it still allows observation of increases or decreases in global stiffness. We also note that the BM around the follicle is about three to six times softer than the BM of the *Drosophila* corneal lens, where as it is much stiffer than the BM (<1 kPa) of the eye disc (Kim et al., 2014; Lavanya Devi et al., 2016). Comparison between these studies and ours is difficult owing to the differences in the geometry of the probes, in the depth of tissue indentation, and in the composition (presence of specific proteins) of the BM (Janssens and Gehring, 1999). Our study infers that the BM of follicles can be considered relatively stiff, since it is stiffer than muscle (elastic modulus E>10 kPa), which presents an intermediate stiffness between lung (E<0.5 kPa) and bones (E>1000 kPa) (Barnes et al., 2017; Butcher et al., 2009). Finally, we observed a difference in BM stiffness in a decellularised context.

Development (2017) 144, 4350-4362 doi:10.1242/dev.152652

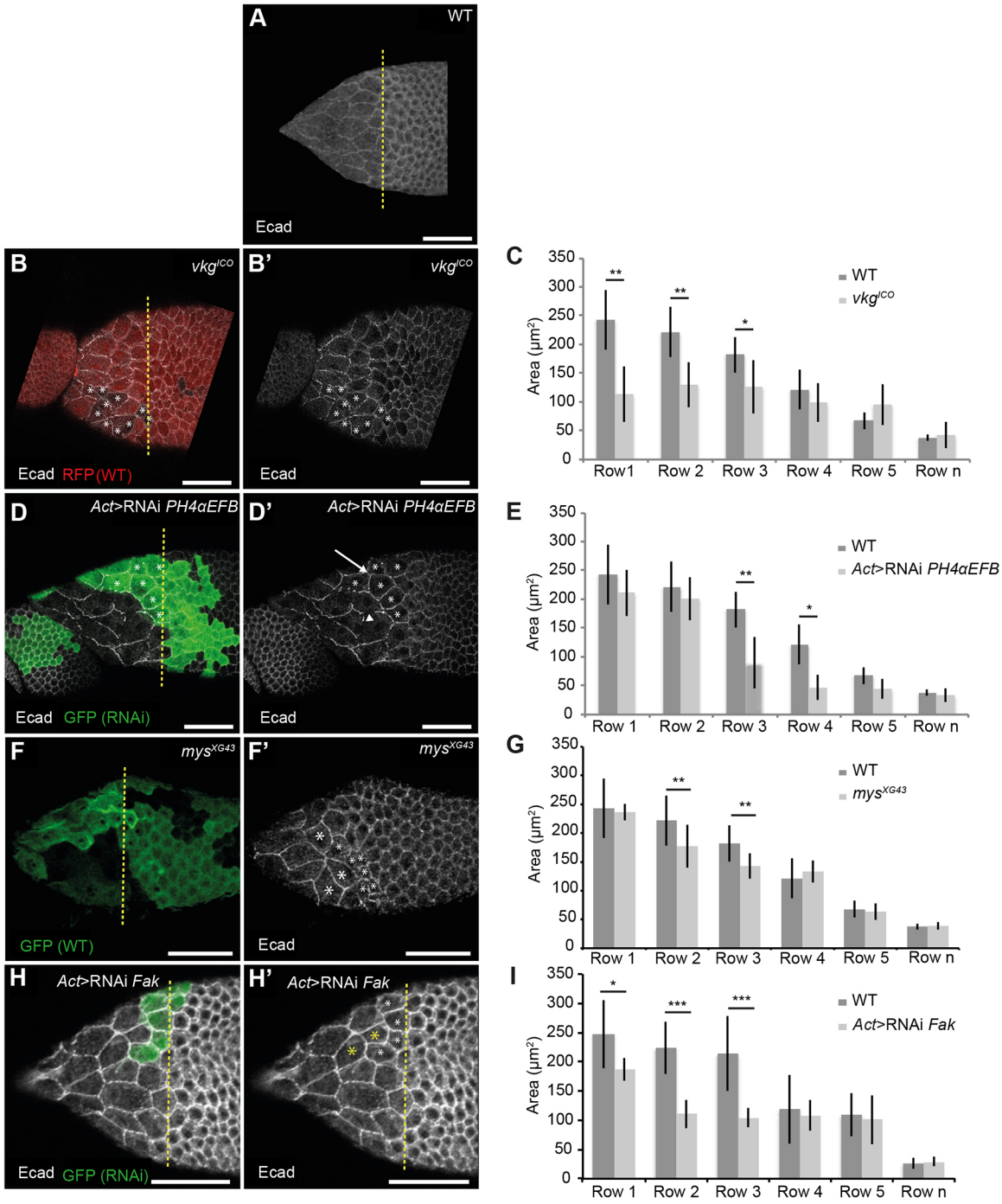

Fig. 6. Cell flattening depends on interactions with the BM. The yellow dotted line marks the row of StCs undergoing flattening. Asterisks indicate mutant cells. (A) WT follicle at mid stage 9 (n=14). (B,B′) Follicle with *vkg*^{ICO} cells with a reduced apical surface compared with WT (n=12). (D,D′) Follicle with cells expressing RNAi against *PH4αEFB* (n=21), with delayed adherens junction remodelling (arrow) compared with WT (arrowhead). (F,F′) Follicle with *mys*^{XG43} cells with a reduced apical surface compared with WT (n=17). Mutant cells are not elongated along the A/P axis (large asterisks). (H,H′) Follicle with cells expressing RNAi against *Fak*, presenting a reduced apical surface (n=9) and preventing elongation of the WT cells (large yellow asterisks) located anteriorly to the clone. (C,E,G,I) Apical surface (area) from WT, *vkg*^{ICO} (C), *PH4αEFB* RNAi (E), *mys*^{XG43} (G) or *Fak* RNAi (I) cells as a function of the row. Twenty cells per row from five to ten mid-stage 9 follicles were measured. Error bars indicate s.e.m. *P<0.05, **P<0.01, ***P<0.005, t-test. Scale bars: 20 µm.

This probably reflects the change of mechanical properties of the BM components between a tense and a relaxed environment.

An important aspect of AFM is that it is a non-invasive method, which allows the visualisation of multiple areas within the same sample. Indeed, obtaining matrices with multiple measurement points is of importance when the sample studied is likely to be heterogeneous. This was especially appropriate to our model, as it has been described that BM incorporates fibrils during follicle development. By combining confocal microscopy with the different modes (QNM mode and Ramp module of the Contact mode) of AFM, we were able to determine that these fibrils are stiffer than the surrounding BM. Fibrils are formed in between the lateral sides of epithelial cells and

Development (2017) 144, 4350-4362 doi:10.1242/dev.152652

then are laid on the BM (Isabella and Horne-Badovinac, 2016). This indicates that the fibrils are not on the outside surface of the BM but are embedded into it. It remains possible, therefore, that not all of the fibrils are detected with an indentation depth of 50 nm.

We and others have shown that BM production and deposition increase during rotation (Bilder and Haigo, 2012; Isabella and Horne-Badovinac, 2015a, 2016). It is likely that the incorporation of new BM material is responsible for the increase in stiffness. Alternative possibilities would be that BM stiffness increases because of the rotation itself (the rotation could help the integration of BM materials, for instance) or because of the cessation of follicular cell division, which occurs at stage 6. Our data do not favour these hypotheses, since stiffness increases while follicular cells divide and occurs in the absence of rotation.

It has been proposed that fibrils create a corset that constrains follicles to growth mainly along the A/P axis. On one hand, our data validate this model since we show that fibrils are stiffer than the surrounding regions and that the presence of linear-oriented structures is likely to be important for follicle elongation. Indeed, although the BM around *fat2* mutant follicles is stiff and heterogeneous, it is not structured in linear patterns, suggesting that spatial organisation of BM mechanical properties is a key parameter for follicle elongation. On the other hand, we show that the size and the density of fibrils may not be the sole parameters involved in the strengthening of the corset, since the increase in stiffness also applies to BM without fibrils and since fibril length varies. Importantly, our data do not exclude an alternative model for follicle elongation that relies on a BM with soft extremities and a stiff central area. A recent paper supports this model (Crest et al., 2017). However, we note that the measurements on *fat2* mutants differ between their study and ours. We found that the BM of *fat2* is, on average, stiffer than that of the WT. The main difference between our approach and theirs is that they probed only a few points, whereas we probed matrices of up to 100 points. We thus revisited our measurements by taking only one force curve from the centre of each matrix, and this lower sampling provides results that are more similar to theirs. A low sampling could also explain the difference in BM stiffness reported in the two studies for the WT [for instance, for a stage 7 follicle: 70 kPa for Crest et al. (2017) versus 250 kPa for this study]. Our 10×10 matrix measurements are likely to obtain values for fibrils in a more spatially representative manner. Our conclusion is that it is necessary to measure extended domains to be able to fully characterise BMs that present spatial heterogeneity. Finally, as AFM measurements are not absolute, differences in raw force curve analyses may also occur, which could partly explain the differences between studies.

The possibility to probe the sample at different positions is crucial to detect variations that can be correlated with biological processes, potentially opening up exploration of the relationship between epithelial morphogenesis, BM remodelling and BM stiffness. Our data provide such an example, as remodelling of the BM structure at stage 9 is rapid (within a couple of hours) and local, with the generation of a gradient of stiffness above the epithelial cells that are instructed by Dpp to flatten. Additionally, interactions with the basal side of the follicular cells through Integrin are also required for cell flattening, confirming that it is an active process. It is important to note that, although BM softens over the StC, its stiffness must be maintained above a certain threshold to prevent round follicles and reduced cell flattening. Indeed, StCs expressing RNAi against *vkg* do not flatten properly, and BM stiffness is very low. Understanding cell flattening thus requires insight into the mechanisms by which Dpp softens the BM basally and how this regulates Integrin signalling or adhesion, but also controls adherens junction remodelling apically (Brigaud et al., 2015). One possibility is through induction of the expression of metalloproteases, which are known to alter Coll IV or DE-cadherin (Lafever et al., 2017).

To conclude, although an increasing number of studies indicate that epithelial morphogenesis depends on internal forces, our analysis shows that understanding the constraint provided by BMs is equally important to shape cells and tissues. Deciphering the mechanical properties of the BM will provide valuable information to help understand epithelial morphogenesis in growing organs.

MATERIALS AND METHODS

Fly stocks and clone generation

Canton S was used as WT. Other fly stocks were: vkg^{G454} (allele containing a GFP protein trap in the Col IV α2 chain Viking, which we refer as Coll IV::GFP in the text; Morin et al., 2001); Trol::GFP (referred to here as Pcan::GFP) (Morin et al., 2001), LanB1::GFP (Morin et al., 2001), endogenous YFP-Rab10 (Dunst et al., 2015), *UAS-vkg-RNAi* (VDRC no. 111668 KK); *UAS-PH4αEFB-RNAi* (TRIP no. HMS00835); *UAS-Fak-RNAi* (VDRC no. 17957); *UAS-pcan-RNAi* (BL29440; Pastor-Pareja and Xu, 2011); vkg^{ICO} FRT40A/CyO (Haigo and Bilder, 2011); mys^{XG43} FRT101/FM7 (Bunch et al., 1992); $fat2^{103C}$/TM6B (Viktorinová et al., 2009); *P*(*UAS-tkv*^{Q199D}) (referred to as TkvA), *P*(*UAS-Dad.T*) (Bangi and Wharton, 2006); and *tj-Gal4* (Li et al., 2003) flies. For further details, see the supplementary Materials and Methods.

Follicle staining and staging

The following antibodies were used: mouse anti-GFP (1:500; Sigma-Aldrich, G6539), goat anti-GFP (1:1000; Abcam, ab5450), rat anti-E-cadherin (1:200; DSHB), rabbit anti-Trol (1:2000) (Friedrich et al., 2000) and rabbit anti-CG25C (1:500), which detects the α1 chain of Coll IV (Van De Bor et al., 2015). Once stained (see the supplementary Materials and Methods), the follicles were staged by calculating the ratio between the length of the oocyte (lo) and the follicle (lf) and according Spradling (1993). Follicles expressing Dad are considered as mid-stage 9 based on the progression of StC flattening (i.e. on the presence of non-flattened, flattening and flattened cells). As StC flattening is delayed in such follicles, they have a larger lf than WT mid-stage 9 follicles. Follicles expressing TkvA are considered at stage 8 based on their lf, which is similar to that of WT stage 8, although cell flattening has already started in TkvA-expressing follicles. For details of Coll IV quantification and morphometric analysis, see the supplementary Materials and Methods.

Mechanical and chemical treatments of follicles

To obtain decellularised BM, follicles were fixed on a Petri dish coated with poly-L-lysine and then cut along the A/P axis with a razor blade.

Collagenase (1000 units/ml CLSP, Worthington Biochemical) was added to a final volume of 200 µl. The reactions were stopped with 10 mM L-cysteine. The ROCK inhibitor Y-27632 (Sigma-Aldrich) was added to a final concentration of 100 µM.

Confocal and electron microscopy

Details of confocal, scanning and transmission electron microscopy of follices are provided in the supplementary Materials and Methods.

Atomic force microscopy (AFM)

Freshly dissected follicles were fixed on a Petri dish coated with poly-L-lysine and recovered with filtrated Schneider medium. Follicles were kept for 1 h maximum before being discarded. For all early stages (prior to stage 8), only one stiffness matrix was obtained per follicle. Analysis of BM stiffness during follicle development was thus performed on different follicles, as follicle development takes 3 days.

AFM indentation experiments were carried out with a Catalyst Bioscope (Bruker Nano Surface, Santa Barbara, CA, USA) that was mounted on an optical macroscope (MacroFluo, Leica) using a 10× objective (Mitutuyo). A NanoScope V controller and NanoScope software version 8.15 (Bruker) were utilised. All quantitative measurements were performed using standard

Development (2017) 144, 4350-4362 doi:10.1242/dev.152652

pyramidal tips (DNP-10, Bruker AFM probes); the tip radius is given by the manufacturer as 20 nm. The spring constant of cantilevers was measured using the thermal tuning method (Hutter and Bechhoefer, 1993; Lévy and Maaloum, 2002) and ranged from 0.03-0.12 N/m. The deflection sensitivity of cantilevers was calibrated against a clean silicon wafer. All experiments were made under Schneider medium at room temperature and the standard cantilever holder for operation in liquid was used. Follicles were dissected from the ovaries. The lower side of the sample was adhered to a Petri dish using poly-L-lysine. The Petri dish was positioned on an *xy* motorised stage and held by a magnetic clamp. Then, the AFM head was mounted on the stage and an approximated positioning with respect to the cantilever was performed using the optical macroscope.

To record surface topology and to create an elastic modulus map, the PeakForce QNM AFM mode was used. The basis of material property mapping with PeakForce QNM is the ability of the system to acquire and analyse individual force curves from each tap that occurs during the imaging process. In this mode, the probe is oscillated at low frequency (0.5 kHz), capturing a force curve each time the AFM tip taps on the sample surface. The maximum force during imaging was 3 nN. For each sample, the topography and elastic modulus images were collected from different locations over regions 5×5 to 20×20 μm^2, at a digital resolution of 64×64 to 256×256 pixels. The 0.3 Hz scanning rate was used.

To record force curves, the Ramp module of the Contact mode was used. The basis of material property measurement with the Ramp module is the ability of the system to acquire individual force curves at discrete points targeted manually by eye. Each AFM measurement consists of the acquisition of 100 force curves extracted as 10×10 matrices with indentation points spaced 150 nm apart, unless otherwise stated. The stiffness is calculated for an indentation depth of 50 nm, unless otherwise specified. In the case of mutant conditions leading to a thinner BM, the values are unlikely to represent the stiffness of the BM alone. Results are presented with grids: each small square corresponds to the analysis of one force-indentation curve. Values are colour coded. The use of a colour scale enables the visualisation of stiffness values from small (blue) to high (red). Matrices are represented with either a common colour scale, which allow comparison between them, or with a specific colour scale that allows better visualisation of differences within the matrices.

Although the QNM method allows the establishment of a topographic or rigidity map, the determination of elastic modulus is less accurate than with the Ramp module of the Contact mode, for which the maximum force used is controlled and the raw force curves include data from more points. On the other hand, the Contact mode is slow.

For both techniques, the elastic modulus is derived from the force-indentation curves using the Hertz–Sneddon model (Sneddon, 1965). This is an appropriate model when the indentation depth is smaller than the sample to be measured (Ogbonna and Needleman, 2011; Oommen and Van Vliet, 2006; Santos et al., 2012), which is the case here: the indentation depth is less than 50 nm for a BM that has a thickness of 80 nm at stage 6 to 180 nm at stage 10 (Spradling, 1993). It assumes a rigid cone indenting a flat surface:

$$F = (2/\pi).(E_s/(1-\nu_s^2)) \cdot \tan(\alpha) \cdot \delta^2, \quad (1)$$

where F is the force from the force curve, E_s is the Young's modulus, ν is the Poisson's ratio, α is the half-angle of the indenter, and δ is the indentation.

We assumed that our sample is perfectly incompressible so that the Poisson's ratio is 0.5. However, since neither the Poisson's ratio nor the tip shape is accurately known, we report in this work only an 'apparent' Young's modulus (Ea).

Statistical analysis

Data are reported as mean±s.e.m. Statistical analysis was performed using R software (RStudio), with alpha levels for all statistical tests set to 5%.

Acknowledgements

We thank the Developmental Studies Hybridoma Bank (DSHB) and Bloomington Drosophila Stock Center for flies and reagents; Lyon Bio Image and Arthrotools of SFR Bioscience (UMS3444/US8), and A. Seigneur for technical support; S. Bogdan, S. Baumgartner, Sally Horne-Badovinac and S. Eaton for flies; X. Wang for use of the Rho kinase inhibitor; V. Van De Bor for flies and discussion; and F. Ruggiero and P. Das for critical comments on the manuscript.

Competing interests

The authors declare no competing or financial interests.

Author contributions

Conceptualization: A.B., M.G.; Methodology: P.M., A.B.; Validation: P.M., G.R., J.-L.D., L.A.; Formal analysis: J.C., G.R., L.A., M.G.; Investigation: J.C., G.R., J.-L.D., L.A., L.-A.L., M.G.; Writing - original draft: M.G.; Writing - review & editing: P.M., A.B., M.G.; Visualization: G.R., M.G.; Supervision: A.B., M.G.; Project administration: M.G.; Funding acquisition: A.B., M.G.

Funding

This work is supported by the Association Nationale de la Recherche et de la Technologie (ANR) (Blanc 12-SVSE-0023-01, MechInMorph), the Centre National de la Recherche Scientifique and the Ecole Normale Supérieure de Lyon.

Supplementary information

Supplementary information available online at http://dev.biologists.org/lookup/doi/10.1242/dev.152652.supplemental

References

Bangi, E. and Wharton, K. (2006). Dpp and Gbb exhibit different effective ranges in the establishment of the BMP activity gradient critical for Drosophila wing patterning. *Dev. Biol.* **295**, 178-193.

Barnes, J. M., Przybyla, L. and Weaver, V. M. (2017). Tissue mechanics regulate brain development, homeostasis and disease. *J. Cell Sci.* **130**, 71-82.

Bilder, D. and Haigo, S. L. (2012). Expanding the morphogenetic repertoire: perspectives from the Drosophila egg. *Dev. Cell* **22**, 12-23.

Brigaud, I., Duteyrat, J.-L., Chlasta, J., Le Bail, S., Couderc, J.-L. and Grammont, M. (2015). Transforming growth factor β/activin signalling induces epithelial cell flattening during Drosophila oogenesis. *Biol. Open* **4**, 345-354.

Bunch, T. A., Salatino, R., Engelsgjerd, M. C., Mukai, L., West, R. F. and Brower, D. L. (1992). Characterization of mutant alleles of myospheroid, the gene encoding the β subunit of the *Drosophila* PS integrins. *Genetics* **132**, 519-528.

Butcher, D. T., Alliston, T. N. and Weaver, V. M. (2009). A tense situation: forcing tumor progresion. *Nat. Rev. Cancer* **9**, 108-122.

Cetera, M., Ramirez-San Juan, G. R., Oakes, P. W., Lewellyn, L., Fairchild, M. J., Tanentzapf, G., Gardel, M. L. and Horne-Badovinac, S. (2014). Epithelial rotation promotes the global alignment of contractile actin bundles during Drosophila egg chamber elongation. *Nat. Commun.* **5**, 5511.

Crest, J., Diz-Muñoz, A., Chen, D. Y., Fletcher, D. A. and Bilder, D. (2017). Organ sculpting by patterned extracellular matrix stiffness. *Elife* **6**, e24958.

Daley, W. P. and Yamada, K. M. (2013). ECM-modulated cellular dynamics as a driving force for tissue morphogenesis. *Curr. Opin. Genet. Dev.* **23**, 408-414.

Diaz de la Loza, M. C., Díaz-Torres, A., Zurita, F., Rosales-Nieves, A. E., Moeendarbary, E., Franze, K., Martin-Bermudo, M. D. and Gonzáles-Reyes, A. (2017). Laminin levels regulate tissue migration and anterior-posterior polarity during egg morphogenesis in Drosophila article laminin levels regulate tissue migration and anterior-posterior polarity during egg morphogenesis in Drosophila. *Cell Rep.* **20**, 211-223.

Dunst, S., Kazimiers, T., von Zadow, F., Jambor, H., Sagner, A., Brankatschk, B., Mahmoud, A., Spannl, S., Tomancak, P., Eaton, S. et al. (2015). Endogenously tagged rab proteins: a resource to study membrane trafficking in Drosophila. *Dev. Cell* **33**, 351-365.

Fernández-Miñán, A., Martín-Bermudo, M. D. and González-Reyes, A. (2007). Integrin signaling regulates spindle orientation in Drosophila to preserve the follicular-epithelium monolayer. *Curr. Biol.* **17**, 683-688.

Friedrich, M. V. K., Schneider, M., Timpl, R. and Baumgartner, S. (2000). Perlecan domain V of Drosophila melanogaster Sequence, recombinant analysis and tissue expression. *Eur. J. Biochem.* **3159**, 3149-3159.

Golic, K. G. and Lindquist, S. (1989). The FLP recombinase of yeast catalyzes site-specific recombination in the Drosophila genome. *Cell* **59**, 499-509.

Grammont, M. (2007). Adherens junction remodeling by the Notch pathway in Drosophila melanogaster oogenesis. *J. Cell Biol.* **177**, 139-150.

Grammont, M. and Irvine, K. D. (2001). fringe and Notch specify polar cell fate during Drosophila oogenesis. *Development* **128**, 2243-2253.

Haigo, S. L. and Bilder, D. (2011). Global tissue revolutions in a morphogenetic movement controlling elongation. *Science* **331**, 1071-1074.

He, L., Wang, X., Tang, H. L. and Montell, D. J. (2010). Tissue elongation requires oscillating contractions of a basal actomyosin network. *Nat. Cell Biol.* **12**, 1133-1142.

Horne-Badovinac, S. and Powell, K. (2015). Sally Horne-Badovinac: Taking a spin around morphogenesis. *J. Cell Biol.* **210**, 4-5.

Hutter, J. L. and Bechhoefer, J. (1993). Calibration of atomic-force microscope tips. *Rev. Sci. Instrum.* **64**, 1868.

Hynes, R. O. (2014). Stretching the boundaries of extracellular matrix research. *Nat. Rev. Mol. Cell Biol.* **15**, 761-763.
Hynes, R. O. and Naba, A. (2012). Overview of the matrisome-an inventory of extracellular matrix constituents and functions. *Cold Spring Harb. Perspect. Biol.* **4**, a004903.
Isabella, A. J. and Horne-Badovinac, S. (2015a). Building from the ground up: basement membranes in Drosophila development. *Curr. Top. Membr.* **76**, 305-336.
Isabella, A. J. and Horne-Badovinac, S. (2015b). Dynamic regulation of basement membrane protein levels promotes egg chamber elongation in Drosophila. *Dev. Biol.* **406**, 212-221.
Isabella, A. J. and Horne-Badovinac, S. (2016). Rab10-mediated secretion synergizes with tissue movement to build a polarized basement membrane architecture for organ morphogenesis. *Dev. Cell* **38**, 47-60.
Ito, K., Sass, H., Urban, J., Hofbauer, A. and Schneuwly, S. (1997). GAL4-responsive UAS-tau as a tool for studying the anatomy and development of the Drosophila central nervous system. *Cell Tissue Res.* **290**, 1-10.
Janssens, H. and Gehring, W. J. (1999). Isolation and characterization of drosocrystallin, a lens crystallin gene of Drosophila melanogaster. *Dev. Biol.* **207**, 204-214.
Kai, F., Laklai, H. and Weaver, V. M. (2016). Force matters: biomechanical regulation of cell invasion and migration in disease. *Trends Cell Biol.* **26**, 486-497.
Kim, S. N., Jeibmann, A., Halama, K., Witte, H. T., Wälte, M., Matzat, T., Schillers, H., Faber, C., Senner, V., Paulus, W. et al. (2014). ECM stiffness regulates glial migration in Drosophila and mammalian glioma models. *Development* **141**, 3233-3242.
King, R. C. (1970). *Ovarian Development in Drosophila melanogaster*. New York: Academic Press.
Lafever, K. S., Wang, X., Page-McCaw, A., Bhave, G. and Page-McCaw, A. (2017). Both Drosophila matrix metalloproteinases have released and membrane-tethered forms but have different substrates. *Sci. Rep.* **7**, 44560.
Lavanya Devi, A. L., Nongthomba, U. and Bobji, M. S. (2016). Quantitative characterization of adhesion and stiffness of corneal lens of Drosophila melanogaster using atomic force microscopy. *J. Mech. Behav. Biomed. Mater.* **53**, 161-173.
Lévy, R. and Maaloum, M. (2002). Measuring the spring constant of atomic force microscope cantilevers : thermal fluctuations and other methods. *Nanotechnology* **13**, 33-37.
Li, M. A., Alls, J. D., Avancini, R. M., Koo, K. and Godt, D. (2003). The large Maf factor Traffic Jam controls gonad morphogenesis in Drosophila. *Nat. Cell Biol.* **5**, 994-100.
Lo, C.-M., Wang, H.-B., Dembo, M. and Wang, Y.-L. (2000). Cell movement is guided by the rigidity of the substrate. *Biophys. J.* **79**, 144-152.
Milani, P., Gholamirad, M., Traas, J., Arnéodo, A., Boudaoud, A., Argoul, F. and Hamant, O. (2011). In vivo analysis of local wall stiffness at the shoot apical meristem in Arabidopsis using atomic force microscopy. *Plant J.* **67**, 1116-1123.
Milani, P., Mirabet, V., Cellier, C., Rozier, F., Hamant, O., Das, P. and Boudaoud, A. (2014). Matching patterns of gene expression to mechanical stiffness at cell resolution through quantitative tandem epifluorescence and nano-indentation. *Plant Physiol.* **165**, 1399-1408.
Morin, X., Daneman, R., Zavortink, M. and Chia, W. (2001). A protein trap strategy to detect GFP-tagged proteins expressed from their endogenous loci in Drosophila. *Proc. Natl. Acad. Sci. USA* **98**, 15050-15055.
Myllyharju, J. and Kivirikko, K. I. (2004). Collagens, modifying enzymes and their mutations in humans, flies and worms. *Trends Genet.* **20**, 33-43.
Ogbonna, N. and Needleman, A. (2011). Conical indentation of thick elastic spherical shells. *J. Mech. Mater. Struct.* **6**, 443-451.
Oommen, B. and Van Vliet, K. J. (2006). Effects of nanoscale thickness and elastic nonlinearity on measured mechanical properties of polymeric films. *Thin Solid Films* **513**, 235-242.
Ozbek, S., Balasubramanian, P. G., Chiquet-Ehrismann, R., Tucker, R. P. and Adams, J. C. (2010). The evolution of extracellular matrix. *Mol. Biol. Cell* **21**, 4300-4305.
Pastor-Pareja, J. C. and Xu, T. (2011). Shaping cells and organs in Drosophila by opposing roles of fat body-secreted collagen IV and perlecan. *Dev. Cell* **21**, 245-256.
Paszek, M. J. and Weaver, V. M. (2004). The tension mounts: mechanics meets morphogenesis and malignancy. *J. Mammary Gland Biol. Neoplasia* **9**, 325-342.
Pearson, J. R., Zurita, F., Tomás-Gallardo, L., Díaz-Torres, A., Díaz de la Loza, M. del C., Franze, K., Martín-Bermudo, M. D., González-Reyes, A., Lu, P., Weaver, V. et al. (2016). ECM-Regulator timp is required for stem cell niche organization and cyst production in the Drosophila ovary. *PLoS Genet.* **12**, e1005763.
Reinhart-King, C. A., Dembo, M. and Hammer, D. A. (2008). Cell-cell mechanical communication through compliant substrates. *Biophys. J.* **95**, 6044-6051.
Roca-Cusachs, P., Sunyer, R. and Trepat, X. (2013). Mechanical guidance of cell migration: lessons from chemotaxis. *Curr. Opin. Cell Biol.* **25**, 543-549.
Saika, S., Saika, S., Liu, C.-Y., Azhar, M., Sanford, L. P., Doetschman, T., Gendron, R. L., Kao, C.-W. and Kao, W. W.-Y. (2001). TGF beta2 in corneal morphogenesis during mouse embryonic development. *Dev. Biol.* **240**, 419-432.
Santos, J. A. C., Rebêlo, L. M., Araujo, A. C., Barros, E. B. and de Sousa, J. S. (2012). Thickness-corrected model for nanoindentation of thin films with conical indenters. *Soft Mat.* **8**, 4441.
Sneddon, I. N. (1965). The relation between load and penetration in the axisymmetric boussinesq problem for a punch of arbitrary profile. *Int. J. Eng. Sci.* **3**, 47-57.
Spradling, A. C. (1993). Developmental genetics of oogenesis. In *The Development of Drosophila melanogaster* (ed. M. Bate and A. Martinez-Arias), pp. 1-70. Cold Spring Harbor, NY: Cold Spring Harbor Laboratory Press.
Squarr, A. J., Brinkmann, K., Chen, B., Steinbacher, T., Ebnet, K., Rosen, M. K. and Bogdan, S. (2016). Fat2 acts through the WAVE regulatory complex to drive collective cell migration during tissue rotation. *J. Cell Biol.* **212**, 591-603.
Tse, J. R. and Engler, A. J. (2011). Stiffness gradients mimicking in vivo tissue variation regulate mesenchymal stem cell fate. *PLoS ONE* **6**, e15978.
Van De Bor, V., Zimniak, G., Papone, L., Cerezo, D., Malbouyres, M., Juan, T., Ruggiero, F. and Noselli, S. (2015). Companion blood cells control ovarian stem cell niche microenvironment and homeostasis. *Cell Rep.* **13**, 546-560.
Viktorinová, I., König, T., Schlichting, K., Dahmann, C., Viktorinova, I., Konig, T., Schlichting, K. and Dahmann, C. (2009). The cadherin Fat2 is required for planar cell polarity in the Drosophila ovary. *Development* **136**, 4123-4132.
Wei, S. C., Fattet, L., Tsai, J. H., Guo, Y., Pai, V. H., Majeski, H. E., Chen, A. C., Sah, R. L., Taylor, S. S., Engler, A. J. et al. (2015). Matrix stiffness drives epithelial–mesenchymal transition and tumour metastasis through a TWIST1–G3BP2 mechanotransduction pathway. *Nat. Cell Biol.* **17**, 678-688.
Xu, T. and Rubin, G. M. (1993). Analysis of genetic mosaics in developing and adult Drosophila tissues. *Development* **117**, 1223-1237.
Yurchenco, P. D. (2011). Basement membranes: cell scaffoldings and signaling platforms. *Cold Spring Harb. Perspect. Biol.* **3**, a004911.